Correlation of luminescence measurements to the structural characterization of Pr3+-doped HfSiOx

Rémi Demoulin, L. Khomenkova, C. Labbe, F. Gourbilleau, Celia Castro, Philippe Pareige, Etienne Talbot

Correlation of luminescence measurements to the structural characterization of Pr^{3+}-doped $HfSiO_x$

R. Demoulin [a], L. Khomenkova [b,c], C. Labbé [b], F. Gourbilleau [b], C. Castro [a], P. Pareige [a], E. Talbot [a,*]

[a] *Groupe de Physique des Matériaux, Normandie Univ, UNIROUEN, INSA Rouen, CNRS, 76000, Rouen, France*
[b] *CIMAP, Normandie Univ, ENSICAEN, UNICAEN, CEA, CNRS, 6 Boulevard Maréchal Juin, 14050, Caen Cedex 4, France*
[c] *V. Lashkaryov Institute of Semiconductor Physics, 45 Pr. Nauky, 03028 Kyiv, Ukraine and National University of "Kyiv-Mohyla Academy", 2 Skovorody Str., 04070, Kyiv, Ukraine*

A B S T R A C T

Luminescence and structural properties of Pr^{3+} doped $HfSiO_x$ thin layer elaborated by magnetron sputtering have been investigated as a function of the annealing temperature. The emission properties of Pr^{3+} ions were studied using photoluminescence (PL) and cathodoluminescence (CL) spectroscopies. Phase separation between amorphous SiO_2 and crystallized HfO_2 nano-grains occurring in the $HfSiO_x$ matrix has been investigated by atom probe tomography and transmission electron microscopy with particular consideration for the Pr distribution. Both PL and CL measurements evidenced a strong emission originating from Pr^{3+} ions in the visible range for an annealing temperature higher than 950°C. At 950°C, Pr^{3+} ions are clearly located in HfO_2 nano-grains of cubic structure. Regarding PL, no significant changes are observed between 950°C and 1050°C. However, CL measurements revealed new emission peaks in the infrared range after an annealing at 1050°C, corresponding to the appearance of a new orthorhombic crystalline structure of HfO_2 nano-grains in the thin layer. The CL signal evolution as a function of the annealing treatment is discussed in regard to the evolution of structural properties.

1. Introduction

Rare earth (RE) doping paved the way for the development of emerging materials in optoelectronics and photonics [1]. More precisely, the combination of a host matrix with a crystalline phase constitutes a perfect environment for optically active ions in order to take the full advantage of their properties. In the past few years, a strong interest has been paid to the RE^{3+} (Er^{3+}, Ce^{3+}, Tb^{3+}, …) doping of silica or silicon-rich silicon oxide host matrices due to their numerous applications in optic or telecommunication systems [1–4]. However, at high doping concentration, it has been shown that the low solubility of RE ions in silicon oxides conducts to the formation of RE-RE bonding leading to the prevalence of cross relaxation effect, or of chemical clusters in form of RE oxides or silicates [5–8]. In many cases, clustering of RE ions leads to the deterioration of their emission properties and limits their use for novel optical applications [6,8,9].

To replace the silicon oxide as host material for RE-doping, hafnium silicates ($HfSiO_x$) appear as a material of choice and are used in the microelectronic field [10,11]. This interest is caused by their high dielectric constant (k ≈ 11–16), their large bandgap (6.5 eV), their high refractive index and the high interface quality with silicon. Moreover, compared to SiO_2, $HfSiO_x$ matrices have lower phonon frequencies reducing the probability of non-radiative recombination, which makes these materials particularly attractive for the RE-doping. Besides, $HfSiO_x$ systems should present a crystal-like environment favourable to the emission properties of RE ions. In fact, it has been evidenced that in undoped as in doped $HfSiO_x$ matrices, an annealing treatment led to a phase separation between a SiO_2 amorphous phase and a crystalline HfO_2 phase [12–14]. Depending on the fabrication conditions (i.e. annealing treatment, dopant species, dopant concentration …), the HfO_2 phase can appear with monoclinic, tetragonal, cubic or orthorhombic crystal form [15,16]. In pure HfO_2 thin films or nanoparticles, high degree of RE-doping leads to a transition from monoclinic to cubic structure due to formation of oxygen vacancies in the HfO_2 phase to keep the electroneutrality of the crystal lattice [17–19]. Moreover, in some cases of RE-doped HfO_2, a cubic to orthorhombic transition has been observed, generating new ferroelectric properties [20–22]. It is worth noting that the type of HfO_2 crystalline phase affect RE PL spectrum, for

instance, for Eu^{3+} doped HfO_2 nanoparticles, the emission properties of Eu^{3+} ions were found to be strongly dependent on the HfO_2 crystalline nature [19].

Recently, we have crossed deep structural analyses with photoluminescence (PL) measurements of Pr^{3+}-doped $HfSiO_x$ thin films in order to reveal the origin of Pr^{3+} emission [23]. An interesting point of Pr^{3+} ions is their capacity to produce simultaneously blue, green, red and near infrared emissions. In this work, we report the cathodoluminescence properties of Pr^{3+} doped $HfSiO_x$ thin films in both visible and infrared range as a function of their annealing treatments, and compare them with the PL and structural characteristics described recently in Ref 19. In this previous study, we have proposed the mechanism leading to the strong Pr^{3+} PL emission peak (487 nm) and demonstrated an effective energy transfer from oxygen vacancies towards Pr^{3+} ions, being both located in cubic HfO_2 nano-crystallites.

2. Material and methods

Pr^{3+}-doped $HfSiO_x$ thin films were produced on *p*-type (100) Si wafer (2 inches in a diameter) by radio-frequency magnetron co-sputtering of a pure HfO_2 target topped by calibrated 1 cm^2 Si and Pr_6O_{11} chips. The deposition was performed with a RF power density of 0.98 $W.cm^{-2}$ in pure Ar plasma. The Si substrate temperature was kept at 25°C. After deposition, the wafer with the film was cut into smaller pieces (so-called as samples) that were annealed at a temperature T_a of 800°C, 950°C and 1050°C under N_2 flow during 1 h.

Photoluminescence measurements were performed using a Jobin Yvon fluorolog spectrometer with an excitation wavelength of 285 nm from a Xenon arc lamp. PL spectra were recorded at room temperature and corrected of the spectral response of the system. Cathodoluminescence (CL) spectra were acquired at room temperature on a HORIBA HCLUE system mounted on a JEOL 7900F scanning electron microscope. Spectra were recorded in scan mode, in a window of 6×4.3 μm^2, in UV–Vis range (300–1000 nm) and in IR range (1000–1500 nm) using 600 and 150-grooves grating, respectively.

Chemical and structural characteristics of Pr^{3+}-doped $HfSiO_x$ films were investigated by Atom Probe Tomography (APT) using a laser-assisted wide-angle tomographic atom probe (LAWATAP-Cameca)

with a femtosecond UV pulsed laser (λ = 343 nm, P = 20 nJ) and a detector yield of 0.62. The experiments were performed in a vacuum chamber at 10^{-10} mbar, at a temperature of 80 K. APT analyses are based on field evaporation effect produced in a tip-shaped sample with a curvature radius lower than 50 nm. Tip samples were prepared following the lift-out and annular milling process, using a dual beam Zeiss NVision 40 FIB-SEM. The APT data analyses were performed using the home built GPM3Dsoft software.

Scanning transmission electron microscopy (STEM) and selected area diffraction (SAED), were performed on a field emission probe Cs aberration corrected JEOL-ARM200F operating at 200 kV. Cross-section TEM samples were prepared by mechanical polishing and ion argon milling procedures. Reference of the layer orientation has been taken on the Si (100) substrate oriented according the [011] zone axis.

X-Ray diffraction (XRD) measurements were performed on a Philips Xpert MPD device with CuKα radiation at a fixed grazing angle incidence of 0.5°.

3. Results

3.1. Luminescence properties

Fig. 1(a–c) show the CL spectra of Pr^{3+}-doped $HfSiO_x$ thin films in the UV–Vis range for the three different T_a. For each T_a, a signal corresponding to the luminescence emission of Pr^{3+} ions due to intra-4f transitions is observed (Fig. 1(d)). The wavelength and the corresponding transitions of each signal are reported in Table 1. The energy of excitation used during CL measurements should allow a direct excitation of RE^{3+} ions, however, an indirect excitation mechanism via host matrix defects may be also considered.

The sample annealed at 800° evidenced four broad CL bands (Fig. 1 (a)). The first one, centred at 493 nm and with a wide spectral spread (468–519 nm), can be associated with the $^3P_0 \rightarrow {}^3H_4$ transition. This peak is the most intense one in all our CL spectra and presents its maximum, in terms of intensity, after an annealing at 1050°. The second band, in the 520–575 nm range, with one peak located at 540 nm is attributed to the $^3P_0 \rightarrow {}^3H_5$ transition. The third band is broad being detected in the 595–675 nm spectral range. This CL band has two peaks
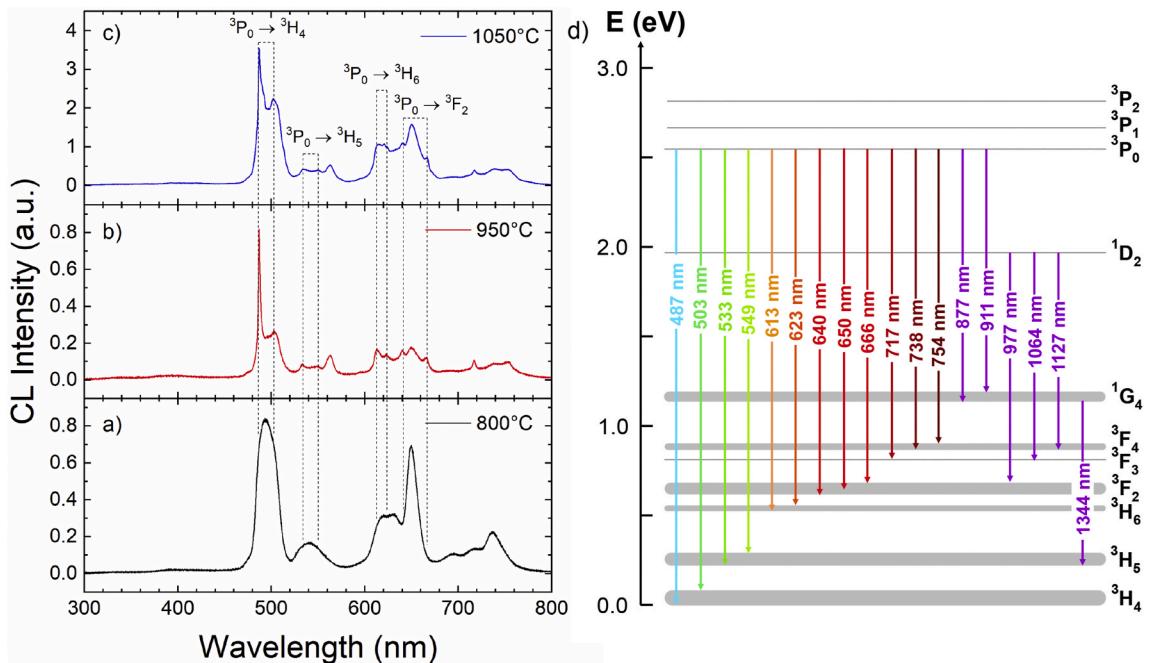

Fig. 1. CL spectra of Pr^{3+}-doped $HfSiO_x$ thin films annealed at (a) 800°C, (b) 950°C and (c) 1050°C in UV–Visible range. Spectra were recorded using a probe current of 1.85 nA with an acceleration voltage of 15 kV. (d) Schematic presentation of intra-4f transitions of Pr^{3+} ions.

Table 1

Electronic transitions observed on CL spectra for different annealing temperatures.

Transition	Wavelength (nm)		
	HfSiO$_x$:Pr - 800°	HfSiO$_x$:Pr - 950°C	HfSiO$_x$:Pr - 1050°C
$^3P_0 \rightarrow {^3H_4}$	493	487–503	487–503
$^3P_0 \rightarrow {^3H_5}$	540	533–549	533–549
$^3P_2 \rightarrow {^3F_2}$	Not detected	563	563
$^3P_0 \rightarrow {^3H_6}$	624	613–623	613–623
$^3P_0 \rightarrow {^3F_2}$	650	640 - 650 - 666	640 - 650 - 666
$^3P_1 \rightarrow {^3F_4}$	694	Not detected	692
$^3P_0 \rightarrow {^3F_3}$	717	717	717
$^3P_0 \rightarrow {^3F_4}$	736	738–754	738–754
$^3P_0 \rightarrow {^1G_4}$	Not detected	Not detected	877 to 911
$^1D_2 \rightarrow {^3F_2}$	Not detected	Not detected	977
$^1D_2 \rightarrow {^3F_3}$	Not detected	Not detected	1064
$^1D_2 \rightarrow {^3F_4}$	Not detected	Not detected	1127
$^1G_4 \rightarrow {^3H_5}$	Not detected	Not detected	1344

at ~625 and 650 nm that can be due to $^3P_0 \rightarrow {^3H_6}$ and $^3P_0 \rightarrow {^3F_2}$ transitions, respectively. The last group is composed of three peaks located at 694, 717 and 736 nm and related to $^3P_1 \rightarrow {^3F_4}$, $^3P_0 \rightarrow {^3F_3}$ and $^3P_0 \rightarrow {^3F_4}$ transitions, respectively. It is worth noting that the major part of CL emission of Pr^{3+} ions emanates from the de-excitation of the $^3P_0$ state. This kind of emission has already been evidenced in other host matrices such as ZnO–SiO$_2$ or ZrO$_2$, in which only the intensity of emission resulting from these transitions seems to vary [24–26].

Strong differences appear between the spectrum recorded for the film annealed at 800° and those treated at higher temperatures. First, if some of the CL bands are located in same spectral ranges, the peaks become to be sharper when T$_a$ increases. This effect can be linked to the effect of spin-orbit and crystal field interactions on the energy levels of Pr^{3+} ions caused by a change of their local environment, allowing clearer separation of the electronic transitions. Hence, it can be ascribed to the crystallization of the HfO$_2$ phase upon heat treatment that is usually observed in this type of materials. The broad CL band, attributed to the $^3P_0 \rightarrow {^3H_4}$, is centred at 495 nm at 800°C. It tends to split into two contributions peaking at 487 and 503 nm at 950°C and 1050°C. Second, the probability of these electronic transitions seems to be influenced by the annealing treatment. In fact, at 950°C, a decrease of the integrated CL intensity is observed before an increase for the highest T$_a$. A phase separation is expected to occur in HfSiO$_x$ matrices towards the formation of two phases SiO$_2$ and HfO$_2$, when T$_a$ reaches values higher than 900°C [12–14]. Thus, in a first step a preferential diffusion of Pr^{3+} ions in the HfO$_2$ phase (evidenced further in section 3.2) may reduce Pr–Pr length and consequently increases the non-radiative recombination rate due to the cross relaxation effect [1], or a partial crystallization of the HfO$_2$ phase can also favored the non-radiative recombination via host matrix defects. In a second step, when T$_a$ reaches 1050°C, the observed increase of CL intensity can be the result of a rearrangement of Pr^{3+} ions in the host matrix or/and a change of Pr^{3+} local environment as well as a recovering of the non-radiative defects.

The PL spectra measured on Pr^{3+}-doped HfSiO$_x$ thin films annealed at 800°C, 950°C and 1050°C are presented in Fig. 2. Unlike the CL results reported above for the layer annealed at 800°C, the corresponding PL spectrum exhibits only a very weak signal at 493 nm which may originates from the $^3P_0 \rightarrow {^3H_4}$ transition of Pr^{3+} ions. The broad PL band observed between 350 and 650 nm was already present in the PL spectrum of undoped sample and was attributed to the response of host material defects under the UV excitation wavelength [27,28]. As Pr^{3+} ions do not present an absorption band at 285 nm, the excitation energy used here does not allow a direct excitation of Pr^{3+} ions. At higher temperatures, the appearance of an intense PL signal attributed to the luminescence of Pr^{3+} ions (Fig. 2(b and c)) shows that the PL of Pr^{3+}-doped HfSiO$_x$ films may be due to an indirect excitation mechanism. According to CL measurements, optically active Pr^{3+} ions are present in all annealed films whatever T$_a$. Then, the absence of sharp
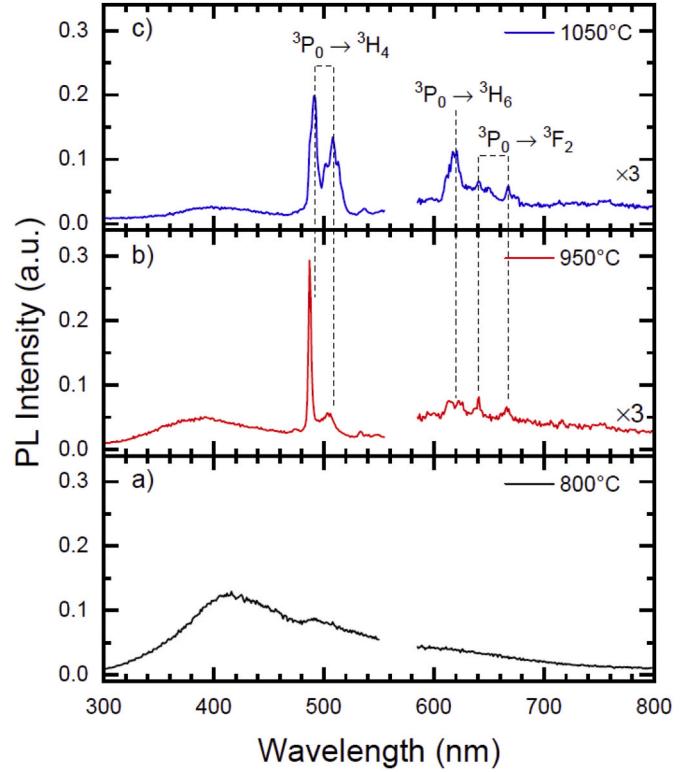

Fig. 2. PL spectra of Pr^{3+} doped HfSiO$_x$ thin films annealed at (a) 800°C, (b) 950°C and (c) 1050°C in UV–Vis range. The excitation wavelength is 285 nm.

Pr^{3+} PL signal at 800°C could be due to (i) the location of Pr^{3+} in an amorphous HfSiO$_x$ host matrix presenting a high rate of non-radiative defects and/or (ii) negligible amount of radiative defect centres in the host matrix acting as sensitizers for Pr^{3+} ions.

The electronic transitions appearing on the 950°C and 1050°C PL spectra are indexed also in Table 2. It is worth noting that the number of PL peaks detected is smaller than that of CL ones. However, all of these peaks were already observed on CL spectra. As for CL measurements, the highest intensity corresponds to the electronic transition $^3P_0 \rightarrow {^3H_4}$ at 487 nm. If the transitions observed at 950°C and 1050°C are the same, the integrated intensity of the PL signal increases and the shape of the PL spectra varies slightly. For instance, for T$_a$ = 1050°C, the second contribution of $^3P_0 \rightarrow {^3H_4}$ transition at 503 nm, tends to split in three different peaks. Contrary to this, both peaks of the $^3P_0 \rightarrow {^3H_6}$ transition, detected at 613 and 623 nm, combine in one single peak observed at 619 nm.

These findings can be explained by the influence of the crystal field surrounding Pr^{3+} ions. In addition to the decomposition of the HfSiO$_x$ matrix, a T$_a$ increase leads to an evolution of the crystalline form of the HfO$_2$ phase, and this can result in a slight modification of the indirect excitation mechanism of Pr^{3+} ions. In fact, it has been proved that a change of the crystalline environment of Pr^{3+} ions can significantly influence their PL properties [29]. It is worth noting that these

Table 2

Electronic transitions observed on PL spectra as a function of the annealing temperature.

Transition	Wavelength (nm)		
	HfSiO$_x$:Pr - 800°C	HfSiO$_x$:Pr - 950°C	HfSiO$_x$:Pr - 1050°C
$^3P_0 \rightarrow {^3H_4}$	493	487–503	487–503
$^3P_0 \rightarrow {^3H_5}$	Not detected	533	533
$^3P_0 \rightarrow {^3H_6}$	Not detected	613–623	619
$^3P_0 \rightarrow {^3F_2}$	Not detected	640–666	640 - 650 - 666

modifications are not observed in CL spectra, in which Pr^{3+} ions emission remains the same in the UV–Visible range. This difference is explained by the higher excitation energy used for CL measurements, Pr^{3+} ions emission changes resulting from the indirect mechanism may be screened by the direct excitation of Pr^{3+} ions.

Concerning the CL spectra measured in the near infrared range, Fig. 3 (a and b) evidence that the emission of Pr^{3+} ions in this range is only visible, with a low intensity, for the thin film annealed at 1050°C. On Fig. 3(a), numerous CL sharp peaks are detected from 870 to 960 nm. These peaks could be attributed to $^3P_0 \rightarrow {}^1G_4$, and $^1D_2 \rightarrow {}^3F_2$ electronic transitions of Pr^{3+} ions. Three other CL peaks can be observed on Fig. 3 (b), two at 1064 and 1127 nm, which may be attributed to the $^1D_2 \rightarrow {}^3F_3$ and $^1D_2 \rightarrow {}^3F_4$ transitions and a last one at 1344 nm that may correspond to the $^1G_4 \rightarrow {}^3H_5$ transition. More, the high resolution of these infrared CL peaks highlights the crystalline nature of Pr^{3+} ions environment. As this CL signal is only detected at 1050°, this should be linked to a change of the crystalline nature of the HfO_2 phase during the thermal treatment.

The influence of the acceleration voltage of the electron beam on CL signal of Pr^{3+}-doped $HfSiO_x$ annealed at 1050°C is represented in Fig. 4. The increase of the acceleration voltage from 4 kV to 30 kV does not affect the overall appearance of the signal and all CL peaks due to electronic transitions of Pr^{3+} observed at 4 kV also appear at 30 kV with similar ratio. In other materials, as in Pr-doped ZrO_2 thin film, an increase of the acceleration voltage results in a significant change of the intensity ratio between the CL bands located at 500 nm and 615 nm [25]. As it is shown on the inset of Fig. 4, the integrated intensity of our film is affected by this acceleration voltage. In fact, the signal intensity reaches a maximum between 15 and 20 kV and tends to decrease at higher voltage. Increasing the acceleration voltage from 4 kV to 30 kV means that the CL signal will be measured at greater depth. As the region of interest consists in a thin film of few hundreds of nanometres, the stable CL intensity measured between 15 and 20 kV evidences that the Pr^{3+}-doped $HfSiO_x$ is homogenous on the entire depth of the sample. Then, the lower intensities measured for lower or higher acceleration voltage show that, in these conditions, the electron beam reaches a smaller part of the thin film.

3.2. Matrix decomposition

Structural characteristics of these three Pr^{3+}-doped $HfSiO_x$ thin layers have been deeply investigated by crossing different analysis methods as Atom Probe Tomography (APT), Transmission Electronic
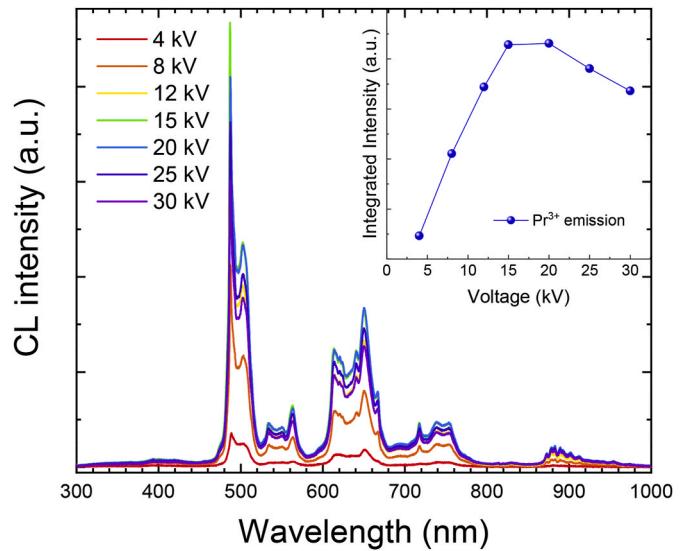
Fig. 4. CL spectra of Pr^{3+}-doped $HfSiO_x$ thin films annealed at 1050°C measured for different acceleration voltages. Spectra were recorded using a probe current of 1.85 nA. The inset corresponds to the evolution of the integrated intensity of the Pr^{3+} signal as a function of the acceleration voltage.

Microscopy (TEM) and X-ray diffraction (XRD) [23,28]. Fig. 5(a–c) display the atomic distributions of Si, Hf and Pr atoms observed in the case of a thin layer annealed at 950°C. In all cases, the atomic distributions are clearly inhomogeneous showing that at high annealing temperature, doped $HfSiO_x$ matrix separates in two distinct phases. This can be confirmed by the STEM HAADF analyses performed on the same sample, showed in Fig. 5(d). In the STEM HAADF picture, the signal intensity is nearly proportional to Z^2. It evidenced the presence of two phases differentiate by two distinct contrasts. Dark contrasted one can be associated to the silicon-based phase and bright contrasted one to the hafnium-based phase evidenced by APT (Fig. 5(a and b)). Crossing both TEM and APT analyses, it was evidenced that these phases could be defined as SiO_2 and HfO_2 [23]. In fact, while concentrations measured on APT analysis in the Si-based phase confirmed the presence of the SiO_2 phase, EELS (electron energy loss spectroscopy) signals detected at the O–K edge in both Si and Hf-based phases clearly characterize the SiO_2 and HfO_2 nature of the different phases [23]. Then, the presence of Si
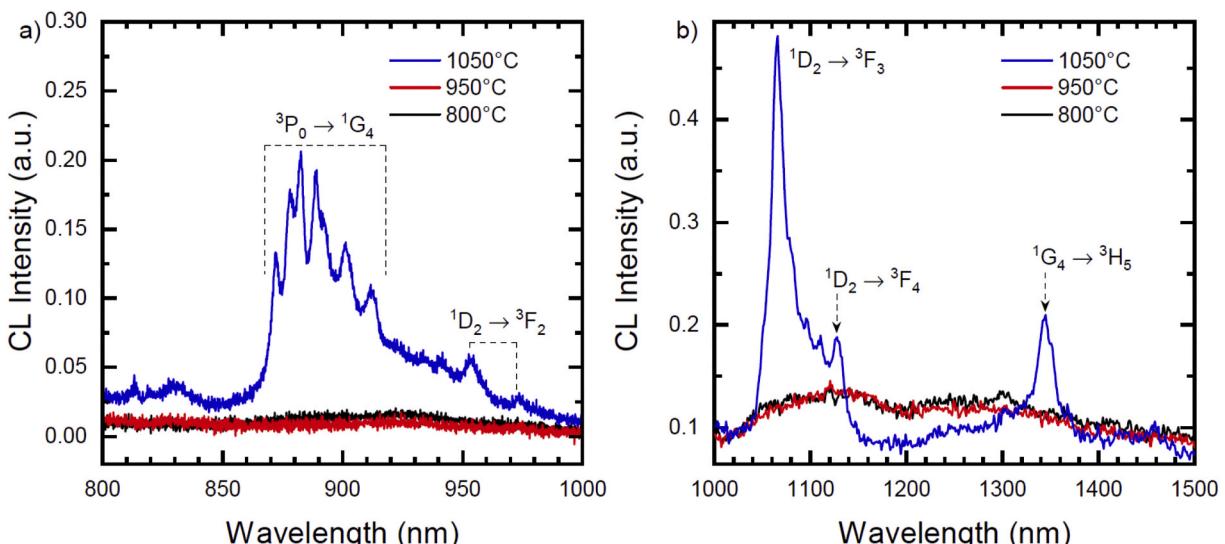
Fig. 3. CL spectra of Pr^{3+}-doped $HfSiO_x$ thin films annealed at 800°C, 950°C and 1050°C in near IR range. Spectra were recorded using an acceleration voltage of 15 kV with (a) a probe current of 1.85 nA and (b) a probe current of 9.47 nA, by consequence measurements of intensities may differ between (a) and (b).
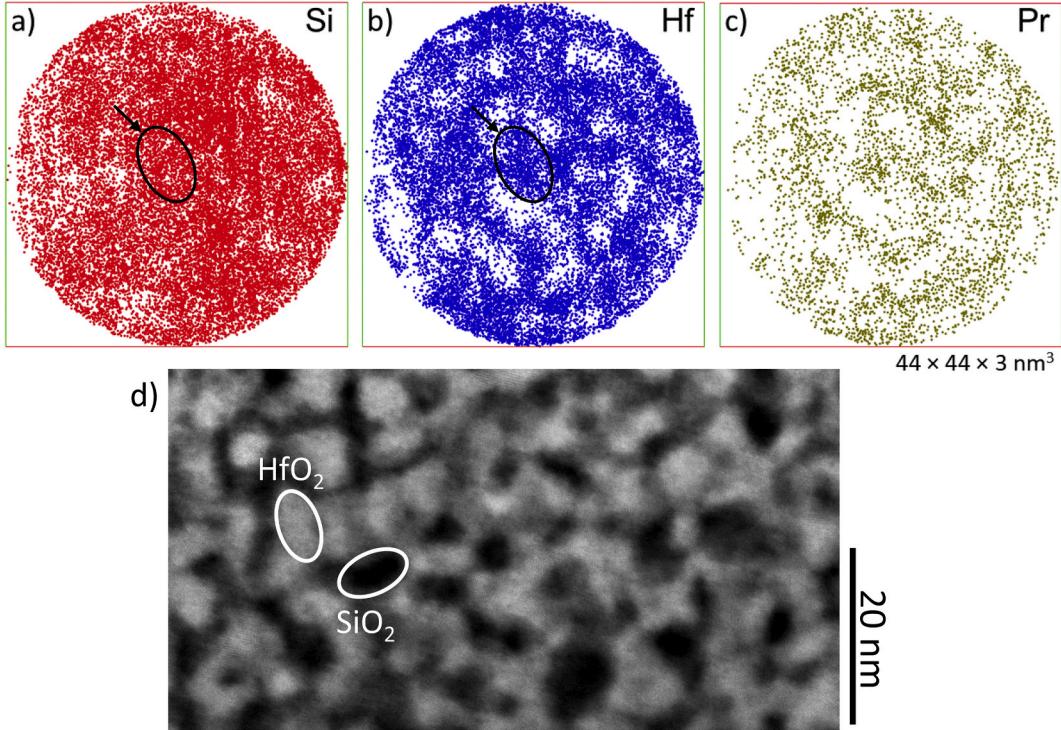
Fig. 5. Three dimensional mappings of (a) Si-, (b) Hf- and (c) Pr-atomic distributions obtained on Pr^{3+}-doped $HfSiO_x$ thin layer annealed at 950°C. The surrounded area shows a part of the HfO_2 phase. It evidences an important artificial inclusion of Si atoms in the HfO_2 phase due to field effect during the APT analysis [30]. (d) STEM HAADF picture of Pr^{3+}-doped $HfSiO_x$ film annealed at 950°C.

atoms in the HfO_2 phase on the 3-D mapping (as shown by the surrounded area on Fig. 5(a and b)) was attributed to the common local magnification effect occurring during the atom probe analysis [30]. Concerning the dopants, the concentration of Pr^{3+} ions in the APT sample can be estimated at about 2.5 at.%. Moreover, these Pr^{3+} ions are only located in the HfO_2 phase, where the Pr^{3+} concentration can reach values from 4 to 5 at.%. Both characteristics, phase separation and location of dopants, are in accordance with conclusions made in the literature on RE ions such as Er^{3+} or Nd^{3+} incorporated in $HfSiO_x$ matrices [31,32]. It is worth noting that similar atomic distributions have been observed on the thin films annealed at 800°C and 1050°C (see supplementary material, Fig. S1) [23]. Indeed, according to atomic distributions, no differences can be evidenced depending on the annealing treatment at mentionned temperatures. Moreover, contrary to the RE incorporation in pure silicon oxide matrix, no Si clustering and/or formation of Si nanoparticles, RE-silicate or RE-oxides have been noticed in the $HfSiO_x$ analysed volumes. Then, with this dopant concentration, the Pr^{3+} doping does not seem to affect the decomposition of the host matrix.

3.3. Crystallization of HfO2

Fig. 6 represents the XRD diffractogram of Pr^{3+}-doped $HfSiO_x$ thin layer as a function of annealing temperature. It can be seen that the $HfSiO_x$ film remains totally amorphous until 950°. However, at 950°C, four intense diffraction peaks are observed at $2\theta = 30.3°$ 35°, 50.3° and 60°. These peaks can respectively be attributed to the (111), (200), (220) and (311) lattice planes of HfO_2 that crystallizes in the cubic fluorite type structure with a space group $F_{m\bar{3}m}$ (JCPDS: n° 53–0550). The stabilization of the cubic form of HfO_2 (c-HfO_2) due to the introduction of RE^{3+} ions is a well-known effect and has already been highlighted throughout the doping of pure HfO_2 thin layers or nanoparticles [17–19,33]. It must be mentioned that, at 1050°C, new diffraction peaks of weak intensity are detected on the XRD
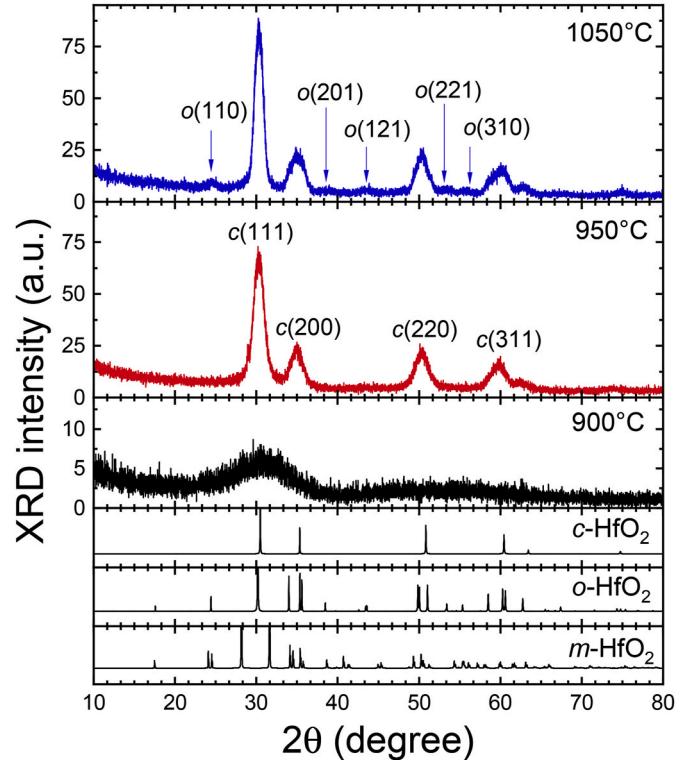

Fig. 6. XRD diffractogram of Pr^{3+}-doped $HfSiO_x$ thin layers as a function of the annealing temperature. Reference pattern correspond to cubic ($F_{m\bar{3}m}$, JCPDS: n° 53–0550), orthorhombic (P_{ca2_1}, JCPDS: n° 83–0808) and monoclinic HfO_2 ($P_{2_1/c}$, JCPDS: n° 43–1017).

diffractogram at $2\theta = 24°$, $38°$, $43.5°$, $53.4°$ and $55.3°$. These peaks show the presence of a new crystalline form of HfO_2, and may be respectively attributed to the (110), (201), (121), (221) and (310) lattice planes of the orthorhombic form of HfO_2 (o-HfO_2) with the space group P_{ca2_1} (JCPDS: n° 83–0808). Comparing the reference diffraction pattern of c-HfO_2 and o-HfO_2, other characteristic signals of o-HfO_2 should be confused with c-HfO_2 signals because of the broadening of the diffraction peaks. Only an increase of the intensity of the peak at 30° is observed and may be due to the (111) lattice plane of the o-HfO_2 which is superimposed with the most intense peak of c-HfO_2.

Fig. 7(a and b) represent the Selected Area Electronic Diffraction (SAED) patterns from both films annealed at 950° and 1050°C. At 950°C, four diffraction rings are clearly identified. The corresponding d_{hkl} spacing are 2.89 Å, 2.51 Å, 1.76 Å and 1.49 Å and are respectively attributed to (111), (200), (220) and (311) lattice planes of c-HfO_2. At 1050°C, the same diffraction rings dominate SAED pattern, however, in agreement with the XRD measurements, new diffraction marks appear. Their d_{hkl} spacing are 3.7 Å and 2.07 Å and correspond respectively to the (110) and (121) lattice planes of o-HfO_2. The low intensities of the characteristic signals of o-HfO_2, in XRD diffractogram as in SAED patterns, evidence that at 1050°C, the o-HfO_2 constitutes only a low content of the crystallized part of the thin film. More, a closer observation by high-resolution STEM (Fig. 7(c and d)) evidences the nano-crystallization of the HfO_2 phase. In these STEM pictures, the size of

nanograins seems to vary from 4 to 6 nm, which correspond to the size observed on APT analyses [23]. In both cases, the measurement of the interplanar spacing confirms the co-existence of c-HfO_2 (Fig. 7(c)) and o-HfO_2 (Fig. 7(d)) nanograins in the film annealed at 1050°C.

Finally, from a pure structural point of view, the evolution of the microstructure of Pr^{3+}-doped $HfSiO_x$ matrix with the annealing temperature may be described in the following way: (i) host material separates in two phases, SiO_2 and HfO_2, and Pr^{3+} ions segregate in the HfO_2 phase, (ii) nano-grains of HfO_2 crystallize in the cubic form, (iii) a cubic to orthorhombic transition of HfO_2 nano-grains occurs.

4. Discussion

In our previous study, we clearly evidenced a link between PL properties and the crystallization of HfO_2 nano-grains in the thin layer [23]. The origin of the Pr^{3+} photoluminescence may be due to an energy transfer between defects states of HfO_2 created by the presence of oxygen vacancies in cubic RE^{3+}-doped HfO_2 and Pr^{3+} ions. In fact, as shown in Fig. 2, the PL signal of Pr^{3+} ions is only detected in the samples annealed at 950°C and 1050°C, which corresponds to the temperature stimulating the crystallization of the HfO_2 phase in these samples. It is worth noting that this PL signal seems to be influenced by the annealing temperature even for temperature higher than 950°C. For instance, some differences are observed on the peaks intensity ratio as well as on
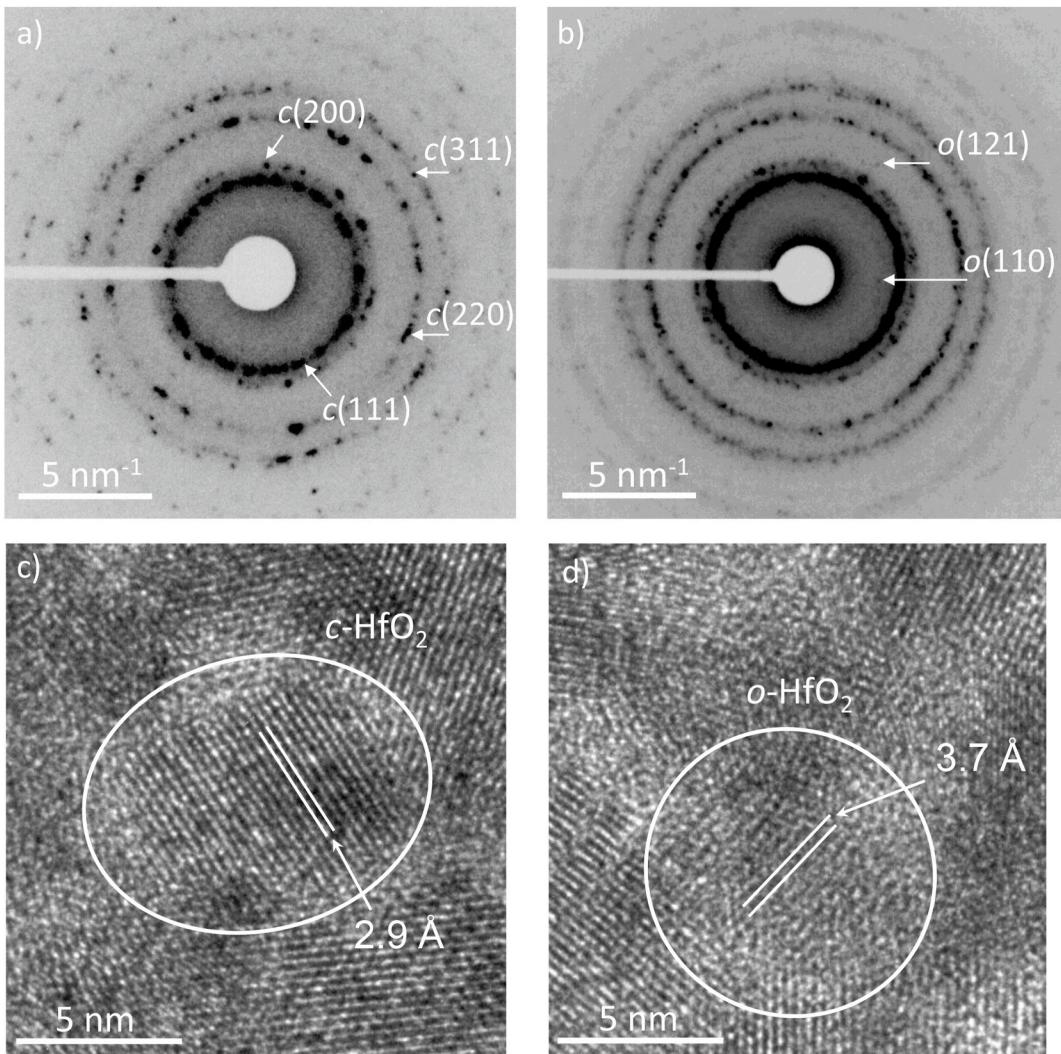

Fig. 7. (a–b) SAED patterns measured on samples annealed at 950°C and 1050°C, respectively. (c–d) High-resolution STEM images obtained on Pr^{3+}-doped $HfSiO_x$ film annealed at 1050°C.

the shape of these peaks (Fig. 2(b and c)). However, from a structural point of view, the analyses detailed above did not allow to highlight significant changes of the film structure to completely understand the PL evolution at high temperature. Another interesting way to bring information on the film structure may consist in studying the CL response of the sample. In fact, the CL signal detected in this kind of material seems to be also correlated to the crystallization of HfO_2 nano-grains. Unlike PL signal, due to the higher energy of the excitation source used for the CL measurements, a CL signal is observed at lower annealing temperature in an amorphous material (Fig. 1). This result clearly shows the presence of Pr in their 3+ valence state. Then, at each T_a, this CL signal should be generated not only by a direct excitation of these ions but also partly by an indirect excitation mechanism via host matrix defects. In these spectra, the crystallization of HfO_2 nano-grains in the host material is characterised by a general enhancement of the CL peaks resolution observed at 950°C and 1050°C. The CL peaks observed at both of these temperatures are very similar in the visible range and originate mainly from the de-excitation of the $^3P_0$ state of Pr^{3+} ions. However, in the sample annealed at 1050°C, significant changes can be evidenced in the infrared range (Fig. 3) with the appearance of CL emission originating from the de-excitation of $^1D_2$ and $^1G_4$ energy level of Pr^{3+} ions. This observation is attributed to a modification of the Pr^{3+} ions environment. As shown by APT analyses, the presence of such new CL peaks at 1050°C is not linked to the clustering of Pr atoms in form of RE-oxides or -silicates. Then, the origin of these highly resolved infrared CL peaks may be explained in part by a change of the crystalline environment around Pr^{3+} ions. Considering SAED pattern (Fig. 7(a and b)) and XRD investigations (Fig. 6), it is clear that the annealing at high temperature ($T_a \geq 950$°C) leads to the formation of c-HfO_2. It must be noted that in these Pr^{3+}-doped $HfSiO_x$ films, the c-HfO_2 can be stabilized with a low Pr^{3+} doping level (~ 2.5 at.%), which correspond to an introduction of 4–5 at.% of Pr^{3+} ions in the c-HfO_2 nanograins. By comparison, the amount of RE^{3+} ions required to stabilize the c-HfO_2 in pure HfO_2 thin film is significantly higher, typically more than 10 at.%, and, by consequence, tend to negatively affect the luminescence properties of RE^{3+} ions in these matrices [17,18]. At 1050°C, both technics evidenced clearly the presence of a new o-HfO_2 phase. It is known that depending on the dopant concentration and/or annealing conditions, a change of crystallinity of the HfO_2 phase can be observed. In fact, some studies have reported a possible phase transition from cubic/tetragonal to monoclinic [34–36] or orthorhombic [21,22] structure of HfO_2, however, the conditions leading to one or the other transition remain misunderstood. In the Pr^{3+}-doped $HfSiO_x$ thin film, the formation of a new o-HfO_2 phase leads to a redistribution of Pr^{3+} ions between c-HfO_2 and o-HfO_2 phases [23]. Thus, the formation of this new HfO_2 polymorph may produce sufficient symmetry changes around Pr^{3+} ions to modify their emission properties. In fact, it is known that Pr^{3+} ions emission properties are easily influenced by the surrounding crystal field [29]. In the present case, the introduction of Pr^{3+} ions in o-HfO_2 bring slight changes on Pr^{3+} emission in visible range. Besides, it may allow generating new transfer path between host matrix and Pr^{3+} ions and/or new relaxation channels between energy levels of Pr^{3+} ions, inducing the possibility to observe radiative de-excitations from $^1D_2$ and $^1G_4$ energy levels in the infrared range.

5. Conclusion

The structural and optical properties of Pr^{3+}-doped $HfSiO_x$ thin layer elaborated by magnetron sputtering were investigated using APT, TEM and XRD experiments as well as PL and CL spectroscopies. It has been shown that the thermal treatment led to a phase separation of the host matrix that is decomposed in two parts, amorphous SiO_2 and crystallized HfO_2 nano-grains. For this latter, the crystallization occurs in the cubic form at 950°C and in the same time a strong PL emission of Pr^{3+} ions is observed in the visible range, originating from the $^3P_0$ energy level. It is worth noting that the structure and the PL emission observed at 950°

and 1050°C are very similar and only slight changes are noted on PL peaks shape. In this case, the use of CL spectroscopy evidenced significant changes between these two samples, marked by the appearance of a new CL emission in the infrared range at 1050°C, originating from $^1D_2$ and $^1G_4$ energy levels of Pr^{3+} ions. The presence of this particular emission at high annealing temperature may confirm a modification of the local crystalline environment of Pr^{3+} ions as evidenced by XRD and TEM studies. Finally, the appearance of the infrared CL emission should be linked to the formation of o-HfO_2 and the redistribution of Pr^{3+} ions between both HfO_2 polymorphs, c-HfO_2 and o-HfO_2.

Declaration of competing interest

The authors declare that they have no known competing financial interests or personal relationships that could have appeared to influence the work reported in this paper.

Appendix A. Supplementary data

Supplementary data to this article can be found online at https://doi.org/10.1016/j.jlumin.2021.118004.

Credit author statement

Rémi Demoulin: Investigation, Formal analysis Writing - original draft, Visualization. Larysa Khomenkova: Investigation, Formal analysis, Writing – review & editing. Christophe Labbé: Investigation, Formal analysis, Writing – review & editing, Fabrice Gourbilleau: Conceptualization, Methodology, Resources, Writing – review & editing. Célia Castro: Investigation, Formal analysis, Writing – review & editing. Philippe Pareige: Validation, Writing – review & editing. Etienne Talbot: Conceptualization, Investigation, Visualization, Supervision, Writing – review & editing.

References

[1] A. Kenyon, Recent developments in rare-earth doped materials for optoelectronics, Prog. Quant. Electron. 26 (4–5) (2002) 225–284, https://doi.org/10.1016/S0079-6727(02)00014-9.

[2] A. Podhorodecki, G. Zatryb, J. Misiewicz, J. Wojcik, P.R.J. Wilson, P. Mascher, Green light emission from terbium doped silicon rich silicon oxide films obtained by plasma enhanced chemical vapor deposition, Nanotechnology 23 (47) (2012) 475707, https://doi.org/10.1088/0957-4484/23/47/475707.

[3] J. Li, O.H.Y. Zalloum, T. Roschuk, C.L. Heng, J. Wojcik, P. Mascher, Light emission from rare-earth doped silicon nanostructures, Advances in Optical Technologies 2008 (2008) 1–10, https://doi.org/10.1155/2008/295601.

[4] S. Cueff, C. Labbé, J. Cardin, J.-L. Doualan, L. Khomenkova, K. Hijazi, O. Jambois, B. Garrido, R. Rizk, Efficient energy transfer from Si-nanoclusters to Er ions in silica induced by substrate heating during deposition, J. Appl. Phys. 108 (6) (2010), 064302, https://doi.org/10.1063/1.3481375.

[5] O. Debieu, D. Bréard, A. Podhorodecki, G. Zatryb, J. Misiewicz, C. Labbé, J. Cardin, F. Gourbilleau, Effect of annealing and Nd concentration on the photoluminescence of Nd^{3+} ions coupled with silicon nanoparticles, J. Appl. Phys. 108 (11) (2010) 113114, https://doi.org/10.1063/1.3510521.

[6] E. Talbot, R. Lardé, P. Pareige, L. Khomenkova, K. Hijazi, F. Gourbilleau, Nanoscale evidence of erbium clustering in Er-doped silicon-rich silica, Nanoscale Research Letters 8 (1). doi:10.1186/1556-276X-8-39.

[7] G. Beainy, J. Weimmerskirch-Aubatin, M. Stoffel, M. Vergnat, H. Rinnert, A. Etienne, P. Pareige, E. Talbot, Atomic scale investigation of Si and Ce-rich nanoclusters in Ce-doped $SiO_{1.5}$ thin films: atomic scale investigation of Si and Ce-rich nanoclusters in Ce-doped $SiO_{1.5}$ thin films, Phys. Status Solidi 12 (12) (2015) 1313–1316, https://doi.org/10.1002/pssc.201510081.

[8] G. Beainy, C. Frilay, P. Gourbilleau, E. Talbot, On the interplay between Si-Er-O segregation and erbium silicate ($Er_2Si_2O_7$) formation in Er-doped SiO_x thin films, J. Alloys Compd. 755 (2018) 55–60, https://doi.org/10.1016/j.jallcom.2018.04.310.

[9] P. Pellegrino, B. Garrido, J. Arbiol, C. Garcia, Y. Lebour, J.R. Morante, Site of Er ions in silica layers codoped with Si nanoclusters and Er, Appl. Phys. Lett. 88 (12) (2006) 121915, https://doi.org/10.1063/1.2190267.

[10] G.D. Wilk, R.M. Wallace, J.M. Anthony, High-k gate dielectrics: current status and materials properties considerations, J. Appl. Phys. 89 (10) (2001) 5243–5275, https://doi.org/10.1063/1.1361065.

[11] J. Choi, Y. Mao, J. Chang, Development of hafnium based high-k materials—a review, Mater. Sci. Eng. R Rep. 72 (6) (2011) 97–136, https://doi.org/10.1016/j.mser.2010.12.001.

[12] H. Kim, P.C. McIntyre, Spinodal decomposition in amorphous metal—silicate thin films: phase diagram analysis and interface effects on kinetics, J. Appl. Phys. 92 (9) (2002) 5094–5102, https://doi.org/10.1063/1.1510590.

[13] S. Stemmer, Y. Li, B. Foran, P.S. Lysaght, S.K. Streiffer, P. Fuoss, S. Seifert, Grazing-incidence small angle x-ray scattering studies of phase separation in hafnium silicate films, Appl. Phys. Lett. 83 (15) (2003) 3141–3143, https://doi.org/10.1063/1.1617369.

[14] J.-P. Maria, D. Wickaksana, J. Parrette, A.I. Kingon, Crystallization in SiO₂–metal oxide alloys, J. Mater. Res. 17 (7) (2002) 1571–1579, https://doi.org/10.1557/JMR.2002.0234.

[15] D.A. Neumayer, E. Cartier, Materials characterization of ZrO₂–SiO₂ and HfO₂–SiO₂ binary oxides deposited by chemical solution deposition, J. Appl. Phys. 90 (4) (2001) 1801–1808, https://doi.org/10.1063/1.1382851.

[16] C.-K. Lee, E. Cho, H.-S. Lee, C. S. Hwang, S. Han, First-principles study on doping and phase stability of HfO₂, Phys. Rev. B 78 (1). doi:10.1103/PhysRevB.78.012102.

[17] S. Kumar, S.B. Rai, C. Rath, Monoclinic to cubic phase transformation and photoluminescence properties in $Hf_{1-x}Sm_xO_2$ (x = 0–0.12) nanoparticles, J. Appl. Phys. 123 (5) (2018), https://doi.org/10.1063/1.5016377, 055108.

[18] S. Kumar, S.B. Rai, C. Rath, Multifunctional role of dysprosium in HfO₂ : stabilization of the high temperature cubic phase, and magnetic and photoluminescence properties, Phys. Chem. Chem. Phys. 19 (29) (2017) 18957–18967, https://doi.org/10.1039/C7CP02800H.

[19] A. Lauria, I. Villa, M. Fasoli, M. Niederberger, A. Vedda, Multifunctional role of rare earth doping in optical materials: nonaqueous sol–gel synthesis of stabilized cubic HfO₂ luminescent nanoparticles, ACS Nano 7 (8) (2013) 7041–7052, https://doi.org/10.1021/nn402357s.

[20] H. Liu, S. Zheng, Q. Chen, B. Zeng, J. Jiang, Q. Peng, M. Liao, Y. Zhou, Structural and ferroelectric properties of Pr doped HfO2 thin films fabricated by chemical solution method, J. Mater. Sci. Mater. Electron. 30 (6) (2019) 5771–5779, https://doi.org/10.1007/s10854-019-00874-4. URL, http://link.springer.com/10.1007/s10854-019-00874-4.

[21] M. Dogan, N. Gong, T.-P. Ma, S. Ismail-Beigi, Causes of ferroelectricity in HfO2-based thin films: an ab initio perspective, Phys. Chem. Chem. Phys. 21 (23) (2019) 12150–12162, https://doi.org/10.1039/C9CP01880H.

[22] Y. Zhou, Y. Zhang, Q. Yang, J. Jiang, P. Fan, M. Liao, Y. Zhou, The effects of oxygen vacancies on ferroelectric phase transition of HfO₂-based thin film from first-principle, Comput. Mater. Sci. 167 (2019) 143–150, https://doi.org/10.1016/j.commatsci.2019.05.041.

[23] R. Demoulin, G. Beainy, C. Castro, P. Pareige, L. Khomenkova, C. Labbé, F. Gourbilleau, E. Talbot, Origin of Pr³⁺ luminescence in hafnium silicate films: combined atom probe tomography and TEM investigations, Nano Futures 2 (3) (2018), https://doi.org/10.1088/2399-1984/aad009, 035005.

[24] G.H. Mhlongo, O.M. Ntwaeaborwa, M.S. Dhlamini, H.C. Swart, K.T. Hillie, Cathodoluminescence properties of SiO₂:Pr³⁺ and ZnO·SiO₂:Pr³⁺ phosphor nanopowders, J. Mater. Sci. 45 (19) (2010) 5228–5236, https://doi.org/10.1007/s10853-010-4563-8.

[25] F. Ramos-Brito, M. García-Hipólito, C. Alejo-Armenta, O. Alvarez-Fragoso, C. Falcony, Characterization of luminescent praseodymium-doped ZrO₂ coatings deposited by ultrasonic spray pyrolysis technique, J. Phys. Appl. Phys. 40 (21) (2007) 6718–6724, https://doi.org/10.1088/0022-3727/40/21/035.

[26] J. Isasi-Marín, M. Pérez-Estébanez, C. Díaz-Guerra, J.F. Castillo, V. Correcher, M. R. Cuervo-Rodríguez, Structural, magnetic and luminescent characteristics of Pr³⁺ -doped ZrO₂ powders synthesized by a sol–gel method, J. Phys. Appl. Phys. 42 (7) (2009), https://doi.org/10.1088/0022-3727/42/7/075418, 075418.

[27] T.-J. Chen, C.-L. Kuo, First principles study of the oxygen vacancy formation and the induced defect states in hafnium silicates, J. Appl. Phys. 111 (7) (2012), https://doi.org/10.1063/1.3702578, 074106.

[28] Y. An, C. Labbé, L. Khomenkova, M. Morales, X. Portier, F. Gourbilleau, Microstructure and optical properties of Pr³⁺-doped hafnium silicate films, Nanoscale Research Letters 8 (1) (2013) 43, https://doi.org/10.1186/1556-276X-8-43.

[29] F. Ramos-Brito, C. Alejo-Armenta, M. García-Hipólito, E. Camarillo, J. Hernández A, H. Murrieta S, C. Falcony, Photoluminescent emission of Pr³⁺ ions in different zirconia crystalline forms, Opt. Mater. 30 (12) (2008) 1840–1847, https://doi.org/10.1016/j.optmat.2007.12.001.

[30] F. Vurpillot, A. Bostel, D. Blavette, Trajectory overlaps and local magnification in three-dimensional atom probe, Appl. Phys. Lett. 76 (21) (2000) 3127–3129, https://doi.org/10.1063/1.126545.

[31] L. Khomenkova, N. Korsunska, C. Labbé, X. Portier, F. Gourbilleau, The peculiarities of structural and optical properties of HfO₂-based films co-doped with silicon and erbium, Appl. Surf. Sci. 471 (2019) 521–527, https://doi.org/10.1016/j.apsusc.2018.11.251.

[32] T. Torchynska, L.G. Vega Macotela, L. Khomenkova, F. Gourbilleau, L. Lartundo Rojas, Annealing impact on emission and phase varying of Nd-doped Si-rich-HfO₂ films prepared by RF magnetron sputtering, J. Mater. Sci. Mater. Electron. 31 (6) (2020) 4587–4594, https://doi.org/10.1007/s10854-020-03010-9.

[33] S. Gálvez-Barboza, L. González, B. Puente-Urbina, E. Saucedo-Salazar, L. García-Cerda, Preparation and characterization of Ce-doped HfO₂ nanoparticles, J. Alloys Compd. 643 (2015) S62–S66, https://doi.org/10.1016/j.jallcom.2014.12.165.

[34] B. Cojocaru, D. Avram, R. Negrea, C. Ghica, V.G. Kessler, G.A. Seisenbaeva, V. I. Parvulescu, C. Tiseanu, Phase control in hafnia: new synthesis approach and convergence of average and local structure properties, ACS Omega 4 (5) (2019) 8881–8891, https://doi.org/10.1021/acsomega.9b00580.

[35] S.V. Ushakov, A. Navrotsky, Y. Yang, S. Stemmer, K. Kukli, M. Ritala, M.A. Leskelä, P. Fejes, A. Demkov, C. Wang, B.-Y. Nguyen, D. Triyoso, P. Tobin, Crystallization in hafnia- and zirconia-based systems, Phys. Status Solidi 241 (10) (2004) 2268–2278, https://doi.org/10.1002/pssb.200404935.

[36] N.D. Afify, G. Dalba, F. Rocca, XRD and EXAFS studies on the structure of Er³⁺-doped SiO₂–HfO₂ glass-ceramic waveguides: Er³⁺-activated HfO₂nanocrystals, J. Phys. Appl. Phys. 42 (11) (2009) 115416, https://doi.org/10.1088/0022-3727/42/11/115416.